
Article:
De domenico, D. and Askes, H. orcid.org/0000-0002-4900-1376 (2016) Computational aspects of a new multi-scale dispersive gradient elasticity model with micro-inertia. International Journal for Numerical Methods in Engineering. ISSN 0029-5981

https://doi.org/10.1002/nme.5278

INTERNATIONAL JOURNAL FOR NUMERICAL METHODS IN ENGINEERING
Int. J. Numer. Meth. Engng 2010; **00**:1–21
Published online in Wiley InterScience (www.interscience.wiley.com). DOI: 10.1002/nme

Computational aspects of a new multi-scale dispersive gradient elasticity model with micro-inertia

Dario De Domenico [1]*, Harm Askes [2]

[1] *Department PAU, University Mediterranea of Reggio Calabria, via Melissari, Reggio Calabria 89124, Italy*
[2] *Department of Civil and Structural Engineering, University of Sheffield, Mappin Street, Sheffield S1 3JD, UK*

SUMMARY

Computational aspects of a recently developed gradient elasticity model are discussed in this paper. This model includes the (Aifantis) strain gradient term along with two higher-order acceleration terms (micro-inertia contributions). It has been demonstrated that the presence of these three gradient terms enables one to capture the dispersive wave propagation with great accuracy. In this paper, the discretisation details of this model are thoroughly investigated, including both discretisation in time and in space. Firstly, the critical time step is derived that is relevant for conditionally stable time integrators. Secondly, recommendations on how to choose the numerical parameters, primarily the element size and time step, are given by comparing the dispersion behaviour of the original higher-order continuum with that of the discretised medium. In so doing, the accuracy of the discretised model can be assessed a priori depending on the selected discretisation parameters for given length scales. A set of guidelines can therefore be established to select optimal discretisation parameters that balance computational efficiency and numerical accuracy. These guidelines are then verified numerically by examining the wave propagation in a one-dimensional bar as well as in a two-dimensional example.

Received . . .

KEY WORDS: Wave dispersion; Gradient elasticity; Multiscale; Finite element methods; Dynamical systems; Generalised continuum

1. INTRODUCTION

Constitutive elastic models for classical continuous media yield a local description of the problem fields whereby the stress at a point depends *uniquely* upon the strain at that point. Such local-type models are consistent with the underlying assumption that the external length-scales and time-scales are much larger than the those of the dominant heterogeneities. Consequently, classical (local) elasticity theory fails to capture phenomena where nonlocal interactions affect the problem outcome, for example at crack-tips or around dislocation cores, for describing size effects, and dispersive wave propagation.

Focusing the attention on wave dispersion, it is usually found that the velocity of the harmonic components reduces as wavelengths approach the physical dimension of the underlying microstructure of a material. These dispersive phenomena cannot be captured unless long-range interactions occurring within the material micro-structure are accounted for in the constitutive model. Therefore, an obvious solution could be to take into account nonlocal interactions between atoms by modelling every single microstructural component individually, which represents the basis

*Correspondence to: Dario De Domenico, Department PAU, University Mediterranea of Reggio Calabria, Reggio Calabria 89124, Italy. Email: dario.dedomenico@unirc.it

of atomistic models. Besides being very difficult to model the exact microstructure for most practical engineering problems, such models are often computationally prohibitive or extremely demanding on memory resources and thus unfeasible to deal with real engineering problems. As an alternative, many enriched (or generalised) continuum theories have been developed to bridge the gap between atomistic models and classical continuum mechanics theory. These theories equip the continuum (macrostructural) formulation with additional length- and time-scales that reflect the underlying material microstructure, see e.g. [2, 4, 7, 12–14, 17, 20] for some comprehensive reviews.

In this paper we restrict our attention to gradient elasticity models, which are a special class of the above generalised theories [1, 4]. These models extend classical elasticity theory by means of additional higher-order spatial derivatives of strains, stresses and/or accelerations in the constitutive equations or in the equations of motion. A class of effective gradient theories for use in dynamics incorporates mixed spatial-temporal derivatives and contains both higher-order strain gradients and higher-order inertia terms. The former are useful to remove singularities, the latter are essential to simulate wave dispersion. The simultaneous presence of both strain gradients and micro-inertia terms has been denoted as *dynamic consistency* in certain previous articles [4–6].

The model dealt with in this paper is an extension of an earlier dynamically consistent model having two gradient contributions [3–5], namely a strain gradient and a micro-inertia term (acceleration gradient). Compared to the latter model, the proposed 'enhanced' model presents a third gradient contribution, namely an additional micro-inertia term multiplying the fourth-order space derivative of the acceleration field in the equations of motion. Therefore, the proposed model incorporates *three* gradient contributions, which are accompanied by three corresponding length scales. The formulation and finite element implementation of such model have already been discussed in [10]. Since the governing partial differential equations are fourth-order in space, spatial discretisation would require $\mathscr{C}^1$-continuity of the interpolation, i.e. continuity of the displacements as well as the much more complicated continuity of the displacement derivatives. To avoid this, the fourth-order equations have been split into a set of two (coupled and symmetric) second-order equations so that $\mathscr{C}^0$-shape functions are sufficient in the finite element implementation. Variationally consistent boundary conditions have been derived and the corresponding discretised equations have been discussed [10]. It has been found that this model is very versatile and provides an improved dispersion behaviour due to the presence of the additional micro-inertia contribution. The inclusion of three free parameters in a gradient elasticity formulation enables a very flexible dispersion curve that can be tailored for a broad variety of engineering materials.

In this paper we do not investigate the physical motivations further but rather we focus on some computational aspects of this model concerning discretisation in space and in time of the underlying equations of motion. Firstly, the continuum equations and the discrete equations of the considered gradient elasticity model are summarised in Section 2. In Section 3 the dispersion relations of the continuum model for compression and shear waves are derived. Some arguments concerning the time integration, the use of explicit or implicit time integrators, as well as the adoption of a lumped or consistent mass matrix formulation are comprised in Section 4. In Section 5 stability aspects are investigated and it is illustrated how the critical time step in the Newmark time integration is affected by the three length scale parameters of the model. Accuracy aspects related to the discretisation are then investigated in Section 6: on the basis of the dispersion analysis of the discretised medium, some guidelines can be established to select optimal values for the element size h and the time step Δt for given length scale parameters. These optimal values can be assessed a priori according to the desired accuracy of the numerical solution as compared to the continuum counterpart. The validity of these guidelines is finally scrutinised in Section 7 by means of two numerical examples concerning the wave propagation in a one-dimensional bar and in a two-dimensional body.

Notation

In the index tensor notation, subscripts denote components with respect to an orthogonal Cartesian coordinate system, say x_i $(i = 1, 2, 3)$; the Einstein summation convention for repeated indices holds. Spatial derivatives are denoted by the comma notation, that is $u_{i,j} = \partial u_i / \partial x_j$. A superimposed dot denotes the derivative with respect to time, that is $\dot{u}_i = \partial u_i / \partial t$. In the matrix-vector notation, boldface lowercase and capital variables denote vectors and matrices, respectively. The

DOI: 10.1002/nme

symbol := means equality by definition. Other symbols will be defined in the text at their first appearance.

2. CONTINUUM EQUATIONS AND SPATIAL DISCRETISATION

Recently, an enhanced gradient elasticity model has been formulated [10]. In this Section we summarise the governing equations of both the higher-order continuum and the spatially discretised counterpart. Such model has been devised based on an earlier dynamically consistent model proposed in [3, 5] and having a strain gradient term as well as a micro-inertia contribution. These two gradients, related to the second-order space derivative of the strain field and of the acceleration field, were accompanied by two material parameters characterising the underlying microstructure and identified as a length scale in statics and in dynamics, respectively.

Motivated by nano-scale experimental evidence on the dispersion characteristics of materials with a lattice structure [22–24], a third additional higher-order inertia contribution has been incorporated in the aforementioned enhanced model. It has been found that such additional micro-inertia term results in a significantly improved dispersion behaviour. Indeed, the associated dispersion curve of this three-parameter model is very flexible, which makes it easy to to tailor it for a broad variety of materials so as to achieve a qualitative match with their corresponding experimental curve—see for instance the simulation of wave propagation in discrete systems and laminates studied in [10].

The model with three parameters formulated in [10] in the hypothesis of homogeneous material (constant density and stiffness tensor) is defined by the following equations of motion

$$\rho\Big(\ddot{u}_i - \alpha\ell^2\ddot{u}_{i,nn} + \beta\ell^4\ddot{u}_{i,jjnn}\Big) = C_{ijkl}\Big(u_{k,jl} - \gamma\ell^2 u_{k,jlnn}\Big) \tag{1}$$

where C_{ijkl} is a fourth-order tensor representing the material stiffness, u_i represent the displacement field and ρ is the mass density. In the sequel we will restrict our attention to isotropic materials for which $C_{ijkl} = \lambda\delta_{ij}\delta_{kl} + \mu\delta_{ik}\delta_{jl} + \mu\delta_{il}\delta_{jk}$, δ_{ij} being Kronecker's delta and λ, μ the Lamé constants. For reasons of dimensional consistency, in (1) the three gradient terms are accompanied by three distinct factors related to the length scale ℓ characterising the underlying material microstructure. The three coefficients α, β, γ *adjust* the relative magnitudes between the various length scales appearing in the strain gradient term and in the micro-inertia contributions. The $\gamma\ell^2$-term represents the gradient enrichment of the one parameter Aifantis 1992 strain gradient theory [1, 2, 21], whereas the earlier dynamically consistent model of [3, 5] is captured by the simultaneous presence of the $\alpha\ell^2$ and $\gamma\ell^2$-terms. Compared to the latter model, an additional term $\beta\ell^4$ appears in the equations of motion (1) multiplying the fourth-order space derivative of the acceleration field. Therefore, the proposed model is defined by *three* independent parameters that are three length scales representing the underlying material microstructure. Procedures to link these three constitutive coefficients to micro-structural properties for a few simple mechanical problems have been discussed in [10].

By inspection of Eq. (1) it emerges that the governing differential equations contains fourth-order spatial derivatives of the u_i unknowns (not only the displacements but also the accelerations). With regard to numerical implementations, this would require shape functions that are $\mathscr{C}^1$-continuous. Although this requirement might be met by using Hermitian $\mathscr{C}^1$ finite elements [26], discontinuous Galerkin methods [11], meshless methods [6] or, alternatively, by discretising multiple fields [25], a simpler approach has been adopted in [10]. According to the latter approach, the fourth-order differential equations are recast, via an operator split, into a set of two second-order differential equations so that a standard finite element implementation with $\mathscr{C}^0$-continuous interpolation functions suffices. To this aim, an auxiliary variable, identified as the *microscopic displacement field* u_i^m, has been introduced in addition to the *macroscopic displacement field* $u_i \equiv u_i^M$ entering Eq. (1). These two displacement fields are related to each other by the differential relation $u_i^M - \gamma\ell^2 u_{i,nn}^M = u_i^m$. The fourth-order differential equations (1) are then rearranged as a set of two coupled and symmetric second-order differential equations in u_i^m and u_i^M as follows (see [10] for the full

DOI: 10.1002/nme

derivation)

$$\rho\left[\left(\frac{\alpha}{\gamma}-\frac{\beta}{\gamma^2}\right)\ddot{u}_i^m-\frac{\beta\ell^2}{\gamma}\ddot{u}_{i,nn}^m-\left(\frac{\alpha}{\gamma}-\frac{\beta}{\gamma^2}-1\right)\ddot{u}_i^M\right]=C_{ijkl}\,u_{k,jl}^m \tag{2a}$$

$$\rho\left[-\left(\frac{\alpha}{\gamma}-\frac{\beta}{\gamma^2}-1\right)\ddot{u}_i^m+\left(\frac{\alpha}{\gamma}-\frac{\beta}{\gamma^2}-1\right)\ddot{u}_i^M-\left(\alpha-\frac{\beta}{\gamma}-\gamma\right)\ell^2\ddot{u}_{i,nn}^M\right]=0\,. \tag{2b}$$

By virtue of the formulation given by Eqs. (2), the additional β term does not imply any additional computational cost as compared to the earlier dynamically consistent model (i.e. with regard to the spatial discretisation and the resulting finite element implementation). The proposed formulation may therefore be considered as an enhanced version of the earlier dynamically consistent model, the latter being retrieved for a zero value of the β term.

As regards the finite element implementation of Eqs. (2), discretisation of the micro- and macro-displacements $\mathbf{u}^m$ and $\mathbf{u}^M$ is carried out with shape functions $\mathbf{N}^m$ and $\mathbf{N}^M$, respectively. Then, the weak form of the equations is considered, integration by parts performed and, finally, the semi-discretised format of equations (i.e. discretised in space but continuous in time) are obtained as follows

$$\begin{bmatrix}\mathbf{M}_{11} & -\mathbf{M}_{12}\\ -\mathbf{M}_{12}^T & \mathbf{M}_{22}\end{bmatrix}\begin{bmatrix}\ddot{\mathbf{d}}^m\\ \ddot{\mathbf{d}}^M\end{bmatrix}+\begin{bmatrix}\mathbf{K}_{11} & \mathbf{0}\\ \mathbf{0} & \mathbf{0}\end{bmatrix}\begin{bmatrix}\mathbf{d}^m\\ \mathbf{d}^M\end{bmatrix}=\begin{bmatrix}\mathbf{f}_{\text{ext}}\\ \mathbf{0}\end{bmatrix} \tag{3}$$

where $\mathbf{d}^m$ and $\mathbf{d}^M$ are the nodal displacements associated to the continuum displacement fields $\mathbf{u}^m$ and $\mathbf{u}^M$, respectively, and the matrix blocks entering expression (3) are defined as

$$\mathbf{M}_{11}=\int_\Omega \mathbf{N}^{mT}\rho\left(\frac{\alpha}{\gamma}-\frac{\beta}{\gamma^2}\right)\mathbf{N}^m\mathrm{d}\Omega+\sum_{\xi=x,y,z}\int_\Omega\frac{\partial\mathbf{N}^{mT}}{\partial\xi}\rho\frac{\beta\ell^2}{\gamma}\frac{\partial\mathbf{N}^m}{\partial\xi}\mathrm{d}\Omega \tag{4a}$$

$$\mathbf{M}_{12}=\int_\Omega \mathbf{N}^{mT}\rho\left(\frac{\alpha}{\gamma}-\frac{\beta}{\gamma^2}-1\right)\mathbf{N}^M\mathrm{d}\Omega \tag{4b}$$

$$\mathbf{M}_{22}=\int_\Omega \mathbf{N}^{MT}\rho\left(\frac{\alpha}{\gamma}-\frac{\beta}{\gamma^2}-1\right)\mathbf{N}^M\mathrm{d}\Omega+\sum_{\xi=x,y,z}\int_\Omega\frac{\partial\mathbf{N}^{MT}}{\partial\xi}\rho\left(\alpha-\frac{\beta}{\gamma}-\gamma\right)\ell^2\frac{\partial\mathbf{N}^M}{\partial\xi}\mathrm{d}\Omega \tag{4c}$$

$$\mathbf{K}_{11}=\int_\Omega \mathbf{B}^{mT}\mathbf{C}\mathbf{B}^m\mathrm{d}\Omega \tag{4d}$$

$$\mathbf{f}_{\text{ext}}=\int_\Gamma \mathbf{N}^{mT}\mathbf{t}\,\mathrm{d}\Gamma. \tag{4e}$$

In expressions (4), $\mathbf{B}^m=\mathbf{L}\mathbf{N}^m$, where $\mathbf{L}$ is a differential operator that relates strains and displacements such that $\boldsymbol{\varepsilon}^m=\mathbf{L}\mathbf{u}^m$. Moreover, $\mathbf{t}=[t_x,t_y,t_z]^T$ are the user-prescribed tractions on the Neumann part Γ_n of the boundary expressed as $\mathbf{t}=\mathbf{N}^T\left(\mathbf{C}\mathbf{L}\mathbf{u}^m+\rho\frac{\beta\ell^2}{\gamma}\nabla\ddot{\mathbf{u}}^m\right)$, where ∇ denotes the gradient operator and the matrix $\mathbf{N}$ contains the components of the outward normal vector $\mathbf{n}=[n_x,n_y,n_z]^T$ to the boundary Γ; note the non-standard addition to the tractions which is in line with earlier gradient theories [3, 5]. Due to the symmetric format of Eqs. (2) (i.e. the coefficient multiplying $\ddot{u}_i^M$ in (2a) is equal to the coefficient multiplying $\ddot{u}_i^m$ in (2b)), the system matrices are symmetric in the corresponding finite element implementation. It can be seen that the system matrices are also positive-definite provided that $\alpha>\frac{\beta}{\gamma}+\gamma$. Time integration of Eqs. (3) is discussed in Section 4.

3. DISPERSION ANALYSIS OF THE CONTINUUM MODEL

In order to analyse the dispersive properties of Eqs. (2), two-dimensional wave propagation is studied with reference to a plane strain configuration. Both displacement fields u_i^m and u_i^M are

DOI: 10.1002/nme

expressed in terms of a dilatation potential Φ and a distortion potential Ψ as

$$u_x^m = \Phi_{,x}^m + \Psi_{,y}^m \qquad \text{and} \qquad u_y^m = \Phi_{,y}^m - \Psi_{,x}^m \tag{5a}$$

$$u_x^M = \Phi_{,x}^M + \Psi_{,y}^M \qquad \text{and} \qquad u_y^M = \Phi_{,y}^M - \Psi_{,x}^M \,. \tag{5b}$$

Substituting expressions (5) into Eqs. (2a) and (2b) one obtains, respectively

$$\begin{bmatrix} \frac{\partial}{\partial x} \\ \frac{\partial}{\partial y} \end{bmatrix} \left\{ \rho \left[\left(\frac{\alpha}{\gamma} - \frac{\beta}{\gamma^2} \right) (\ddot{\Phi}^m - \ddot{\Phi}^M) + \ddot{\Phi}^M - \frac{\beta \ell^2}{\gamma} (\ddot{\Phi}_{,xx}^m + \ddot{\Phi}_{,yy}^m) \right] - (\lambda + 2\mu)(\Phi_{,xx}^m + \Phi_{,yy}^m) \right\} +$$
$$\begin{bmatrix} \frac{\partial}{\partial y} \\ -\frac{\partial}{\partial x} \end{bmatrix} \left\{ \rho \left[\left(\frac{\alpha}{\gamma} - \frac{\beta}{\gamma^2} \right) (\ddot{\Psi}^m - \ddot{\Psi}^M) + \ddot{\Psi}^M - \frac{\beta \ell^2}{\gamma} (\ddot{\Psi}_{,xx}^m + \ddot{\Psi}_{,yy}^m) \right] - \mu \left(\Psi_{,xx}^m + \Psi_{,yy}^m \right) \right\} = \begin{bmatrix} 0 \\ 0 \end{bmatrix} \tag{6a}$$

$$\begin{bmatrix} \frac{\partial}{\partial x} \\ \frac{\partial}{\partial y} \end{bmatrix} \left\{ \rho \left[\left(\frac{\alpha}{\gamma} - \frac{\beta}{\gamma^2} - 1 \right) (\ddot{\Phi}^M - \ddot{\Phi}^m) - \left(\alpha - \frac{\beta}{\gamma} - \gamma \right) \ell^2 (\ddot{\Phi}_{,xx}^M + \ddot{\Phi}_{,yy}^M) \right] \right\} +$$
$$\begin{bmatrix} \frac{\partial}{\partial y} \\ -\frac{\partial}{\partial x} \end{bmatrix} \left\{ \rho \left[\left(\frac{\alpha}{\gamma} - \frac{\beta}{\gamma^2} - 1 \right) (\ddot{\Psi}^M - \ddot{\Psi}^m) - \left(\alpha - \frac{\beta}{\gamma} - \gamma \right) \ell^2 \left(\ddot{\Psi}_{,xx}^M + \ddot{\Psi}_{,yy}^M \right) \right] \right\} = \begin{bmatrix} 0 \\ 0 \end{bmatrix} \tag{6b}$$

Since Eqs. (6) must hold for *arbitrary* (non-zero) waves, it follows that the expressions in braces must vanish. Therefore, compressive waves are studied in terms of the dilatation potentials Φ^m and Φ^M via the following equations

$$\rho \left[\left(\frac{\alpha}{\gamma} - \frac{\beta}{\gamma^2} \right) (\ddot{\Phi}^m - \ddot{\Phi}^M) + \ddot{\Phi}^M - \frac{\beta \ell^2}{\gamma} (\ddot{\Phi}_{,xx}^m + \ddot{\Phi}_{,yy}^m) \right] - (\lambda + 2\mu)(\Phi_{,xx}^m + \Phi_{,yy}^m) = 0 \tag{7a}$$

$$\rho \left[\left(\frac{\alpha}{\gamma} - \frac{\beta}{\gamma^2} - 1 \right) (\ddot{\Phi}^M - \ddot{\Phi}^m) - \left(\alpha - \frac{\beta}{\gamma} - \gamma \right) \ell^2 (\ddot{\Phi}_{,xx}^M + \ddot{\Phi}_{,yy}^M) \right] = 0 \tag{7b}$$

Since all the model parameters, including the three coefficients characterising the length scale terms as well as the Lamé constants, are assumed to be constant coefficients, Eqs. (7) admit solutions given by two general harmonic functions

$$\Phi^m(x,t) = \hat{\Phi}^m \exp(\mathrm{i}\,(k_x x + k_y y - \omega t)) \tag{8a}$$

$$\Phi^M(x,t) = \hat{\Phi}^M \exp(\mathrm{i}\,(k_x x + k_y y - \omega t)) \tag{8b}$$

where $\hat{\Phi}^m$ and $\hat{\Phi}^M$ are amplitudes, i the imaginary unit, ω the angular frequency whilst k_x and k_y are the wave numbers in the x and y direction. Substituting these two trial functions into Eqs. (7) yields

$$\omega^2 \left(\frac{\alpha}{\gamma} - \frac{\beta}{\gamma^2} - 1 \right) \hat{\Phi}^M + \hat{\Phi}^m \left[c_p^2 k^2 - \omega^2 \left(\frac{\alpha}{\gamma} - \frac{\beta}{\gamma^2} (1 - \gamma k^2 \ell^2) \right) \right] = 0 \tag{9a}$$

$$\left(\frac{\alpha}{\gamma} - \frac{\beta}{\gamma^2} - 1 \right) \left(\hat{\Phi}^m - \hat{\Phi}^M (1 + \gamma k^2 \ell^2) \right) \omega^2 = 0 \tag{9b}$$

in which $k = \sqrt{k_x^2 + k_y^2}$ represents the modulus of the wave vector in two dimensions and $c_p = \sqrt{(\lambda + 2\mu)/\rho}$ is the long wave length limit of the compressive wave velocity. From Eq. (9b) one obtains a relation between the two amplitudes as $\hat{\Phi}^M = \hat{\Phi}^m / (1 + \gamma k^2 \ell^2)$. Eq. (9a) can then be elaborated as

$$\hat{\Phi}^m \left[\omega^2 \left(\frac{\alpha}{\gamma} - \frac{\beta}{\gamma^2} - 1 \right) \frac{1}{1 + \gamma k^2 \ell^2} + c_p^2 k^2 - \omega^2 \left(\frac{\alpha}{\gamma} - \frac{\beta}{\gamma^2} (1 - \gamma k^2 \ell^2) \right) \right] = 0 \tag{10}$$

that can be rewritten in dimensionless form by introducing the dimensionless wave number $\chi := k\ell$

$$\frac{c^2}{c_p^2} = \frac{1 + \gamma \chi^2}{1 + \alpha \chi^2 + \beta \chi^4} . \tag{11}$$

DOI: 10.1002/nme

For the shear waves the same procedure is employed with reference to the distortion potentials Ψ^m and Ψ^M in (6), and the following expression is found

$$\frac{c^2}{c_s^2} = \frac{1+\gamma\chi^2}{1+\alpha\chi^2+\beta\chi^4} \tag{12}$$

where $c_s = \sqrt{\mu/\rho}$ is the velocity of the shear waves with infinite wavelength. The comparison betweens Eqs. (11) and (12) shows that the dispersion curves for the compressive and shear waves have the same shape, the only difference being the constant by which they are scaled. The dispersion relations (11) and (12) are such that the strain gradient term accelerates while the micro-inertia terms decelerate the higher wave numbers compared to the lower wave numbers. Consequently, for $\alpha > \gamma - \beta\chi^2$ the higher wave numbers travel slower than the lower wave numbers. The one-dimensional case may be retrieved from Eq. (11) for a zero value of the Poisson's ratio ν, leading to Lamé constants $\lambda = 0$, $\mu = E/2$ (E being the Young's modulus) and, thus, $c_p \equiv c_e = \sqrt{E/\rho}$ where c_e represents the one-dimensional bar velocity of classical elasticity. Note that unlike the dynamically consistent model with two length scale parameters [3, 5, 9], the case $\alpha = \gamma$ does not lead to a non-dispersive medium due to the presence of the β term in the denominator of Eqs. (11) and (12).

4. TIME INTEGRATION AND MASS MATRIX FORMULATION ARGUMENTS

Equations (3) are discretised in space but still continuous in time. For the time discretisation of Eqs. (3) one of the most widely used family of implicit methods is the Newmark family [15, 18]. As well known, if a constant time step Δt is considered such that two subsequent time instants are denoted as $t^j = j\Delta t$ and $t^{j+1} = (j+1)\Delta t$, the (numerical approximation of the) nodal velocities and nodal displacements at time t^{j+1} are expressed as

$$\dot{\mathbf{d}}^{(j+1)} = \dot{\mathbf{d}}^{(j)} + \Delta t \left[(1-\gamma_n)\, \ddot{\mathbf{d}}^{(j)} + \gamma_n\, \ddot{\mathbf{d}}^{(j+1)} \right] \tag{13a}$$

$$\mathbf{d}^{(j+1)} = \mathbf{d}^{(j)} + \Delta t\, \dot{\mathbf{d}}^{(j)} + \frac{\Delta t^2}{2} \left[(1-2\beta_n)\, \ddot{\mathbf{d}}^{(j)} + 2\beta_n \ddot{\mathbf{d}}^{(j+1)} \right] \tag{13b}$$

where the Newmark parameters γ_n and β_n set the accuracy, stability and numerical damping of the time integration scheme. The Newmark method is unconditionally stable if $\gamma_n \geq 1/2$ and $\beta_n \geq 1/4\,(\gamma_n + 1/2)^2$. The Newmark family contains as special cases many well-known and widely used methods, for instance the unconditionally stable constant average acceleration variant (trapezoidal rule) is retrieved for $\gamma_n = 1/2$ and $\beta_n = 1/4$. Other well-known members of the Newmark family are the linear acceleration scheme ($\gamma_n = 1/2$ and $\beta_n = 1/6$) and the Fox-Goodwin scheme ($\gamma_n = 1/2$ and $\beta_n = 1/12$), which are only conditionally stable. Stability of the conditionally stable algorithms is discussed in Section 5.

Due to the structure of the spatially discretised system of equations (3), it is more convenient to solve in terms of accelerations. The time-discretised counterpart of Eqs. (3) according to expressions (13) reads

$$\begin{bmatrix} \mathbf{M}_{11} + \beta_n \Delta t^2\, \mathbf{K}_{11} & -\mathbf{M}_{12} \\ -\mathbf{M}_{12}^T & \mathbf{M}_{22} \end{bmatrix} \begin{bmatrix} \ddot{\mathbf{d}}^{m(j+1)} \\ \ddot{\mathbf{d}}^{M(j+1)} \end{bmatrix} = \begin{bmatrix} \mathbf{f}_{\text{ext}}^{(j+1)} - \mathbf{f}_{\text{int}}^{(j)} \\ \mathbf{0} \end{bmatrix} \tag{14}$$

with

$$\mathbf{f}_{\text{int}}^{(j)} = \mathbf{K}_{11} \left(\mathbf{d}^{m(j)} + \Delta t\, \dot{\mathbf{d}}^{m(j)} + \frac{\Delta t^2}{2} (1-2\beta_n)\, \ddot{\mathbf{d}}^{m(j)} \right) \tag{15}$$

which is used for the subsequent simulations in a recursive fashion.

As an alternative, an explicit Runge-Kutta algorithm may be adopted. We consider a vector $\mathbf{d} = [\mathbf{d}^m, \mathbf{d}^M]^T$ collecting the microscopic and macroscopic displacements so that Eqs. (3) can be expressed in compact form as

$$\mathbf{M}\, \ddot{\mathbf{d}}(t) + \mathbf{K}\, \mathbf{d}(t) = \mathbf{F}(t). \tag{16}$$

DOI: 10.1002/nme

These n second-order differential equations are recast into a set of $2n$ first-order equations as follows

$$\dot{\mathbf{y}}(t) = \mathbf{D_N}\,\mathbf{y}(t) + \mathbf{V_N}\,\mathbf{F}(t) \tag{17}$$

where

$$\mathbf{y} = \begin{bmatrix} \mathbf{d} \\ \dot{\mathbf{d}} \end{bmatrix}; \quad \mathbf{D_N} = \begin{bmatrix} \mathbf{0} & \mathbf{I} \\ -\mathbf{M}^{-1}\mathbf{K} & \mathbf{0} \end{bmatrix}; \quad \mathbf{V_N} = \begin{bmatrix} \mathbf{0} \\ \mathbf{M}^{-1} \end{bmatrix} \tag{18}$$

$\mathbf{0}$ and $\mathbf{I}$ being a n-by-n zero and identity matrices, respectively. Eq. (16) can be handled by explicit Runge-Kutta solvers implemented as software toolbox, e.g. in MATLAB [16].

It is well known that explicit time integration is efficient if the mass matrix is diagonal. However, in line with the arguments of Bennett & Askes [9], the use of a lumped mass matrix is not recommended as this would eliminate all the higher-order effects and would be inappropriate for this format of gradient elasticity. For this reason, consistent mass matrices will be adopted for all the numerical examples in the paper.

5. STABILITY ASPECTS: CRITICAL TIME STEP

Some implicit algorithms of the Newmark family are only conditionally stable. Consequently, the applied time step must be selected smaller than a so-called *critical time step* in order for the simulations to remain numerically stable. The critical time step can be calculated as [15]

$$\Delta t_{\text{crit}} = \frac{\Omega_{\text{crit}}}{\omega_{\text{max}}} \tag{19}$$

in which Ω_{crit} is the critical sampling frequency of the Newmark scheme and ω_{max} is the highest frequency of the total system. A conservative value of the critical time step is evaluated by taking an upper bound of the frequency as $\omega_{\text{max}} = \omega^e_{\text{max}}$ (where ω^e_{max} is the maximum frequency of the individual finite element) in combination with a lower bound of the sampling frequency as $\Omega_{\text{crit}} = 1/\sqrt{\gamma_n/2 - \beta_n}$. The maximum frequency that can be captured by the spatial discretisation depends on the specific element being used (interpolation, type of integration, mass distribution). It can be obtained by solving the homogeneous equivalent expression of Eqs. (16) at element level, which yields the following eigenvalue problem in ω

$$\det[-\omega^2\,\mathbf{M} + \mathbf{K}] = 0. \tag{20}$$

For a two-noded bar element of length h, unitary cross-section and linear shape functions, the element mass matrix and stiffness matrix are given by (cf. Eqs. (3) and (4))

$$\mathbf{M} = \begin{bmatrix} \left(\frac{\alpha}{\gamma} - \frac{\beta}{\gamma^2}\right)\mathbf{M}_c + \frac{\beta\ell^2}{\gamma}\mathbf{M}_g & -\left(\frac{\alpha}{\gamma} - \frac{\beta}{\gamma^2} - 1\right)\mathbf{M}_c \\ -\left(\frac{\alpha}{\gamma} - \frac{\beta}{\gamma^2} - 1\right)\mathbf{M}_c & \left(\frac{\alpha}{\gamma} - \frac{\beta}{\gamma^2} - 1\right)\left(\mathbf{M}_c + \gamma\ell^2\,\mathbf{M}_g\right) \end{bmatrix}, \quad \mathbf{K} = \begin{bmatrix} \mathbf{K}_c & \mathbf{0} \\ \mathbf{0} & \mathbf{0} \end{bmatrix} \tag{21}$$

where $\mathbf{M}_c$ and $\mathbf{K}_c$ are the usual mass matrix and stiffness matrix of classical elasticity, while $\mathbf{M}_g$ is a gradient-enriched contribution to the mass matrix given by

$$\mathbf{M}_c = \frac{\rho h}{6}\begin{bmatrix} 2 & 1 \\ 1 & 2 \end{bmatrix}, \quad \mathbf{K}_c = \frac{E}{h}\begin{bmatrix} 1 & -1 \\ -1 & 1 \end{bmatrix}, \quad \mathbf{M}_g = \frac{\rho}{h}\begin{bmatrix} 1 & -1 \\ -1 & 1 \end{bmatrix}. \tag{22}$$

Inserting these expression into the eigenvalue problem (20) leads to three zero eigenvalues (characterising some rigid body motions) and a non-zero frequency representing the sought ω_{max} value

$$\omega^2_{\text{max}} = \frac{12c_e^2}{h^2}\left(\frac{1 + 12\,\gamma\left(\frac{\ell}{h}\right)^2}{1 + 12\,\alpha\left(\frac{\ell}{h}\right)^2 + 144\,\beta\left(\frac{\ell}{h}\right)^4}\right) \tag{23}$$

where $c_e^2 = E/\rho$. Since in classical elasticity the non-zero eigenfrequency for a two-noded finite element with linear shape functions and a consistent mass distribution is $\omega_c^2 = 12c_e^2/h^2$, relation

DOI: 10.1002/nme

(23) can be regarded as the eigenfrequency of the classical elasticity multiplied with the bracketed correction factor that is related to the gradient effects. It can be observed that such bracketed factor is always positive for any choice of the coefficients α, β, γ provided that these coefficients are positive. This means that the corresponding eigenfrequency is always real, which is an indicator of dynamic stability of the finite element implementation regardless of the relative magnitudes between the three length scale parameters. Inserting (23) into (19), the critical time step is expressed as

$$\Delta t_{\text{crit}} = \frac{h}{c_e\sqrt{6\gamma_n - 12\beta_n}}\sqrt{\frac{1+12\,\alpha\left(\frac{\ell}{h}\right)^2+144\,\beta\left(\frac{\ell}{h}\right)^4}{1+12\,\gamma\left(\frac{\ell}{h}\right)^2}} \tag{24}$$

which is again expressed as the critical time step for classical elasticity (retrieved for $\ell = 0$) multiplied with a correction factor that involves the three length scale material parameters. In order to assess the dispersive behaviour of the material objectively, in the sequel we will ignore the numerical damping by assuming $\gamma_n = 1/2$ throughout. This implies that the effect of numerical damping has no effect on stability. However, if $\gamma_n > 1/2$ the effect of numerical damping would increase the critical time step of conditionally stable Newmark methods, therefore the undamped critical sampling frequency serves as a conservative value when an estimate of the modal damping coefficient is not available [15]. In Fig. 1 we report the normalised critical time step $\Delta t_{\text{crit}}\, c_e/\ell$ in terms of the normalised element size h/ℓ as per Eq. (24) for both the linear acceleration scheme ($\beta_n = 1/6$) and the Fox-Goodwin scheme ($\beta_n = 1/12$). The three length scale material parameters are chosen as $\alpha = 2$, $\beta = 0.5$, $\gamma = 1$.

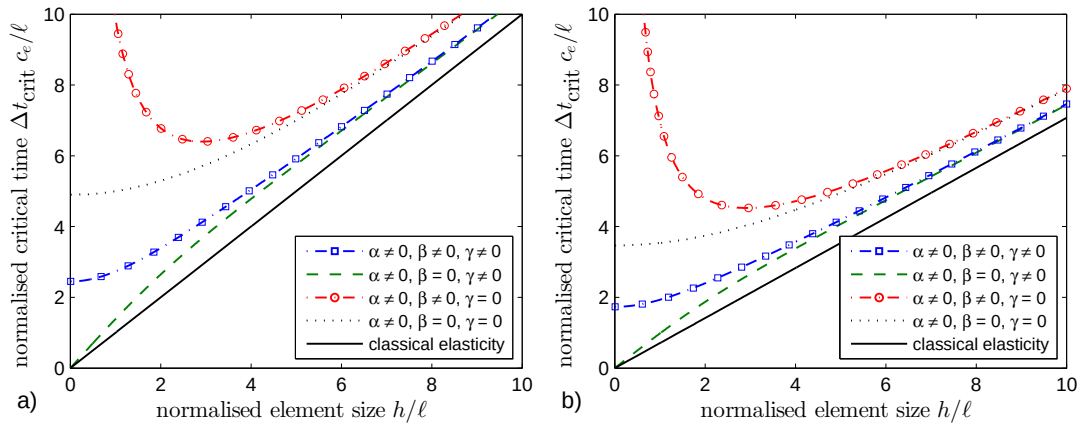

Figure 1. Normalised critical time step *versus* normalised element size as expressed by Eq. (24): a) linear acceleration scheme ($\beta_n = 1/6$); b) Fox-Goodwin scheme ($\beta_n = 1/12$)

From Eq. (24) it can be seen that the limit of the critical time step for infinitely small element size depends on the three length scales as follows

$$\lim_{h\to 0}\Delta t_{\text{crit}} = \begin{cases} \frac{2}{c_e\sqrt{1-4\beta_n}}\sqrt{\alpha\ell^2} & \text{if } \beta = 0 \wedge \gamma = 0 \\ \frac{2}{c_e\sqrt{1-4\beta_n}}\sqrt{\frac{\beta\ell^2}{\gamma}} & \text{otherwise.} \end{cases} \tag{25}$$

The value of Δt_{crit} tends to increase with increasing normalised element size h/ℓ. Moreover, the β term has an increasing effect on the critical time step as compared to the case $\beta = 0$, especially for small element sizes (whereas for large element size the effect of the β tends to reduce). Note also that from Eq. (24), for $\alpha > \gamma$ (strictly speaking, for $\alpha > \gamma - 12\beta\frac{\ell^2}{h^2}$) the critical time step of the gradient elasticity model is *larger* than the critical time step of classical elasticity.

In Section 7 these findings will be verified numerically.

Remark 1

Denoting with $u_1^m, u_2^m, u_1^M, u_2^M$ the four element degrees of freedom (DOFs), namely two

DOI: 10.1002/nme

microscopic displacements and two macroscopic displacements, 1 and 2 being the two nodes of the bar element, the three zero eigenvalues $\omega_1 = \omega_2 = \omega_3 = 0$ are associated with the following three eigenmodes: $\phi_1 \rightarrow u_1^M = 1$ and the remaining three DOFs = 0; $\phi_2 \rightarrow u_2^M = 1$ and the remaining three DOFs = 0; $\phi_3 \rightarrow u_1^m = u_2^m = 1$ and the remaining two DOFs = 0. Of the three eigenvectors, only ϕ_3 can be clearly identified as a rigid body motion in terms of the microscopic displacement field. Actually, eigenvectors ϕ_1 and ϕ_2 are not easily interpreted as the macroscopic and microscopic displacements are related to each other through the expression $u_i^M - \gamma\ell^2 u_{i,nn}^M = u_i^m$. However, eigenmodes 1 and 2 cannot be triggered (which is confirmed by numerical analyses, where these zero eigenmodes play no role). In this context, it is noted that the proposed formulation can only be used in dynamics: Eq. (3) shows that its static reduction is rank-deficient and thus not usable. Therefore, $\omega = 0$ is only of theoretical importance and has no practical implications.

6. ACCURACY ASPECTS: DISCRETE DISPERSION RELATIONS

In this Section the dispersion relations for the model after discretisation in space and in time are derived. In order to assess the accuracy of the discretised model, the dispersion curve of the discretised medium is compared to that of the higher-order continuum discussed in Section 3. On the basis of this comparison, some guidelines can be established to select optimal values for the element size h and the time step Δt (for given material length scale parameters) that balance computational efficiency and numerical accuracy. For simplicity, such guidelines are derived with reference to the one-dimensional case, linear finite elements for the spatial discretisation and the Newmark scheme for the time integration (taking again $\gamma_n = 1/2$ to avoid numerical damping).

6.1. Time discretisation: relation between displacements and accelerations

It can be noted that Eqs. (3) contain both accelerations and displacements, the latter of which are of simpler format. In order to derive the discrete dispersion relations, we eliminate the displacements from the formulation. Following the derivations of Bennett & Askes [9] based on the Newmark algorithm, the displacements and accelerations at three consecutive time instants $j-1$, j and $j+1$ can be related via the following expression

$$d^{(j-1)} + d^{(j+1)} = 2d^{(j)} + \beta_n \Delta t^2\, \ddot{d}^{(j-1)} + (1 - 2\beta_n)\, \Delta t^2 \ddot{d}^{(j)} + \beta_n \Delta t^2 \ddot{d}^{(j+1)} \tag{26}$$

which will be used further on to eliminate the displacements from the formulation and to rewrite the dispersion relations in terms of accelerations only.

6.2. Spatial discretisation: dispersion analysis of the discretised model

For the spatial discretisation of the equations of motion (3) a uniform mesh with element size h is adopted. Consequently, the position of the generic node n is indicated as $x_n = nh$ and the corresponding displacement-type variable is denoted as d_n. The one-dimensional format of the equations of motion (3) can be written by taking into account the element mass matrix and stiffness matrix as expressed by Eqs. (21) and (22). After assembly of the discretised equations, the two equations pertaining to the generic node n involve variables (microscopic and macroscopic displacements and accelerations) of the adjacent nodes $n-1$, n and $n+1$. After a bit of straightforward algebra, they can be written as

$$\tilde{\eta}_1(\ddot{d}_{n-1}^m + \ddot{d}_{n+1}^m) + \tilde{\eta}_2\, \ddot{d}_n^m - \eta_3(\ddot{d}_{n-1}^M + 4\ddot{d}_n^M + \ddot{d}_{n+1}^M) - \eta_5(d_{n-1}^m - 2d_n^m + d_{n+1}^m) = 0 \tag{27a}$$

$$-\eta_3(\ddot{d}_{n-1}^m + 4\ddot{d}_n^m + \ddot{d}_{n+1}^m) + \tilde{\eta}_3(\ddot{d}_{n-1}^M - \ddot{d}_{n+1}^M) + \tilde{\eta}_4\, \ddot{d}_n^M = 0 \tag{27b}$$

DOI: 10.1002/nme

where $\tilde{\eta}_1 = \eta_1 - \eta_2$, $\tilde{\eta}_2 = 4\eta_1 + 2\eta_2$, $\tilde{\eta}_3 = \eta_3 - \eta_4$, $\tilde{\eta}_4 = 4\eta_3 + 2\eta_4$, and the following definitions of the five coefficients η_i $(i = 1, \ldots, 5)$ entering expressions (27) are used

$$\begin{gathered}\eta_1 := \left(\frac{\alpha}{\gamma} - \frac{\beta}{\gamma^2}\right)\frac{h}{6}; \quad \eta_2 := \frac{\beta\ell^2}{\gamma}\frac{1}{h}; \quad \eta_3 := \left(\frac{\alpha}{\gamma} - \frac{\beta}{\gamma^2} - 1\right)\frac{h}{6}; \\ \eta_4 := \left(\frac{\alpha}{\gamma} - \frac{\beta}{\gamma^2} - 1\right)\gamma\ell^2\frac{1}{h}; \quad \eta_5 := \frac{c_e^2}{h}.\end{gathered} \tag{28}$$

The two equations (27) are coupled, therefore for the generic node n at time instant t^j the micro- and macro-accelerations can be expressed by the following general harmonic functions, respectively

$$\ddot{d}_n^{m(j)} = A\exp\left(\mathrm{i}\,k(nh - c\,j\Delta t)\right) \tag{29a}$$

$$\ddot{d}_n^{M(j)} = U\exp\left(\mathrm{i}\,k(nh - c\,j\Delta t)\right) \tag{29b}$$

where A and U are two distinct amplitudes, while the same wave number k and phase velocity c are assumed for the two solutions. The assumptions on the uniform discretisation in space and in time have been used in expressions (29), by which for adjacent nodes and subsequent time steps we can write $\ddot{d}_{n\pm1}^{(j\pm1)} = \ddot{d}_n^{(j)}\exp(\pm\mathrm{i}\,kh)\exp(\mp\mathrm{i}\,kc\Delta t)$ for both d^m and d^M. Substituting the two trial functions (29) into the second discretised equation of motion (27b) (where only accelerations appear) leads to a relation between the two amplitudes as follows

$$U = A\left[\frac{\eta_3\left(2 + \cos(kh)\right)}{2\eta_3 + \eta_4 + (\eta_3 - \eta_4)\cos(kh)}\right]. \tag{30}$$

The goal is now to eliminate the displacements from Eq. (27a). To this aim, we evaluate Eq. (27a) at times t^{j-1} and t^{j+1} and these two expressions are added up. We only focus on the displacement terms multiplying η_5 in the resulting expression that are reported below

$$\left(d_{n-1}^{m(j-1)} + d_{n-1}^{m(j+1)}\right) - 2\left(d_n^{m(j-1)} + d_n^{m(j+1)}\right) + \left(d_{n+1}^{m(j-1)} + d_{n+1}^{m(j+1)}\right). \tag{31}$$

These terms can be eliminated using relation (26) for each bracketed pair of displacements pertaining to the three nodes $n-1$, n and $n+1$. After using relation (26) into (31), some displacement components at time t^j still appear in the resulting equations that are given by $\left(d_{n-1}^{m(j)} - 2d_n^{m(j)} + d_{n+1}^{m(j)}\right)$ multiplied by a factor 2. These displacements can be replaced by acceleration components using again Eq. (27a) evaluated at time t^j, in other words solving Eq. (27a) for the η_5-term. After these mathematical manipulations and some simplifications, Eq. (27a) rewritten in terms of acceleration components only reads

$$\begin{aligned}&\tilde{\eta}_1\big(-2\ddot{d}_{n-1}^{m(j)} + \ddot{d}_{n-1}^{m(j-1)} + \ddot{d}_{n-1}^{m(j+1)} - 2\ddot{d}_{n+1}^{m(j)} + \ddot{d}_{n+1}^{m(j-1)} + \ddot{d}_{n+1}^{m(j+1)}\big) + \tilde{\eta}_2\big(-2\ddot{d}_n^{m(j)} + \ddot{d}_n^{m(j-1)} \\ &\quad + \ddot{d}_n^{m(j+1)}\big) + \eta_3\big(8\ddot{d}_n^{M(j)} - 4\ddot{d}_n^{M(j-1)} - 4\ddot{d}_n^{M(j+1)} + 2\ddot{d}_{n-1}^{M(j)} - \ddot{d}_{n-1}^{M(j-1)} - \ddot{d}_{n-1}^{M(j+1)} \\ &\quad + 2\ddot{d}_{n+1}^{M(j)} - \ddot{d}_{n+1}^{M(j-1)} - \ddot{d}_{n+1}^{M(j+1)}\big) + \eta_5\Big[(2\beta_n\Delta t^2 - \Delta t^2)\big(-2\ddot{d}_n^{m(j)} + \ddot{d}_{n-1}^{m(j)} + \ddot{d}_{n+1}^{m(j)}\big) \\ &\quad - \beta_n\Delta t^2\big(-2\ddot{d}_n^{m(j-1)} + \ddot{d}_{n-1}^{m(j-1)} + \ddot{d}_{n+1}^{m(j-1)} - 2\ddot{d}_n^{m(j+1)} + \ddot{d}_{n-1}^{m(j+1)} + \ddot{d}_{n+1}^{m(j+1)}\big)\Big].\end{aligned} \tag{32}$$

Substituting the harmonic functions (29) into (32) and exploiting Euler's formula $\exp(\pm\mathrm{i}\theta) = \cos(\theta) \pm \mathrm{i}\sin(\theta)$ yields the simplified expression

$$\begin{aligned}&\eta_1\left[-8A\left(2 + \cos(kh)\right)\sin^2\left(\frac{ck\Delta t}{2}\right)\right] + \eta_2\left[-16A\sin^2\left(\frac{kh}{2}\right)\sin^2\left(\frac{ck\Delta t}{2}\right)\right] \\ &+\eta_3\left[8U\left(2 + \cos(kh)\right)\sin^2\left(\frac{ck\Delta t}{2}\right)\right] + \eta_5\left[4A\Delta t^2\left(1 - 2\beta_n + 2\beta_n\cos(ck\Delta t)\right)\sin^2\left(\frac{kh}{2}\right)\right] = 0\end{aligned} \tag{33}$$

DOI: 10.1002/nme

where both the amplitudes A and U appear. To eliminate the amplitudes, the relation (30) between A and U is inserted into (33). Then we use the positions $Y := \sin^2\left(\frac{ck\Delta t}{2}\right)$ and $X := \sin^2\left(\frac{kh}{2}\right)$, from which $\cos\left(ck\Delta t\right) = 1 - 2Y$ and $\cos\left(kh\right) = 1 - 2X$. In this way Eq. (33) can be handled as a linear equation for the Y variable in terms of the X variable, whose solution is given by

$$Y = \frac{X\Delta t^2\eta_5\left[(3-2X)\eta_3 + 2X\eta_4\right]}{2\eta_3\left[\eta_1(2X-3)^2 - 9\eta_3 + 6X(\tilde{\eta}_5 + 2\eta_3)\right] - 4X\eta_1\eta_4(2X-3) - 8X^2\tilde{\eta}_3\tilde{\eta}_5} \tag{34}$$

where $\tilde{\eta}_5 = \eta_2 + \eta_5\beta_n\Delta t^2$. Once the Y variable is evaluated via Eq. (34), the phase velocity c can be derived as follows

$$c = \frac{2\arcsin(\sqrt{Y})}{k\Delta t} = f(k, h, \Delta t, \beta_n, \alpha, \beta, \gamma, \ell, c_e) \tag{35}$$

which is the sought dispersion relation for the model after discretisation in space and in time. Through such relation the phase velocity c is expressed as a function of the wave number k, the discretisation parameters h and Δt, the Newmark constant β_n as well as the three material coefficients α, β, γ related to the length scale ℓ.

6.3. Guidelines to select optimal numerical parameters

Once the discrete dispersion relation (35) is derived, it is interesting to make a comparison with the dispersion curve of the continuum model (11). In so doing, the accuracy of the discretised model can be assessed depending on the selected numerical parameters, more specifically, time step and element size for given length scales. A range of numerical parameters are investigated and the corresponding discretisation error is evaluated, from which one can suggest guidelines to select optimal discretisation parameters that balance computational efficiency and numerical accuracy. Interestingly, and in contrast to classical elasticity, this can be done *a priori*, that is prior to the computer simulation. The dimensionless phase velocity c/c_e is evaluated via Eq. (35) as a function of the dimensionless wave number $k\ell$. We consider different values of dimensionless element size h/ℓ and dimensionless time step $\Delta t c_e/\ell$, as well as different ratios between the three length scale parameters expressed by $r_\alpha = \alpha/\gamma$ and $r_\beta = \beta/\gamma$, and different values of the Newmark parameter β_n.

In Fig. 2 we describe the effect of the discretisation parameters, namely the (dimensionless) element size and time step, on the accuracy of the solution for $r_\alpha = 2$ and $r_\beta = 0.5$. By inspection of Fig. 2 a) and b) one can see that, if a unitary dimensionless time step is adopted, a reasonably good match is obtained up to dimensionless wave numbers $k\ell \approx 2$ for element size $h/\ell = 1.5$, and up to dimensionless wave numbers $k\ell \approx 4$ for element size $h/\ell = 1.0$. Adopting a smaller element size $h/\ell = 0.5$ leads to a very accurate description of the dispersion curve of the continuum model up to dimensionless wave numbers $k\ell \approx 10$ for both the linear acceleration scheme and the constant acceleration scheme. On the other hand, it can be seen that for a fixed dimensionless element size there is no advantage in adopting smaller time steps than an optimal value. In Fig. 2 c) and d) we show the effect of reducing the time step while keeping a unitary dimensionless element size. Interestingly, no significant improvement is observed by comparing the dispersion curve of the continuum model with the discrete dispersion curves obtained for $\Delta t c_e/\ell = 1$ and $\Delta t c_e/\ell = 0.25$, i.e. when the time step is refined by a factor 4. On the contrary, as will be shown below it may be counterproductive to decrease either element size or time step without decreasing the other simultaneously.

The effect of the length scale parameters is analysed in Fig. 3. For the constant acceleration scheme and for fixed values of the (dimensionless) element size $h/\ell = 1$ and time step $\Delta t c_e/\ell = 1$ we compare the dispersion curves of the discrete model with those of the continuum counterpart for different ratios r_α and r_β. Increasing the r_α ratio for fixed r_β does not alter the accuracy of the discrete solution significantly, as the range of wave numbers for which the dispersion curve is captured accurately is basically the same, namely up to $k\ell \approx 3$ for the considered parameters, see Fig. 3 a). Conversely, increasing the r_β ratio for fixed r_α yields an improvement in the prediction of the dispersive behaviour as can be seen in Fig. 3 b). This means that if larger values of the β-related

DOI: 10.1002/nme

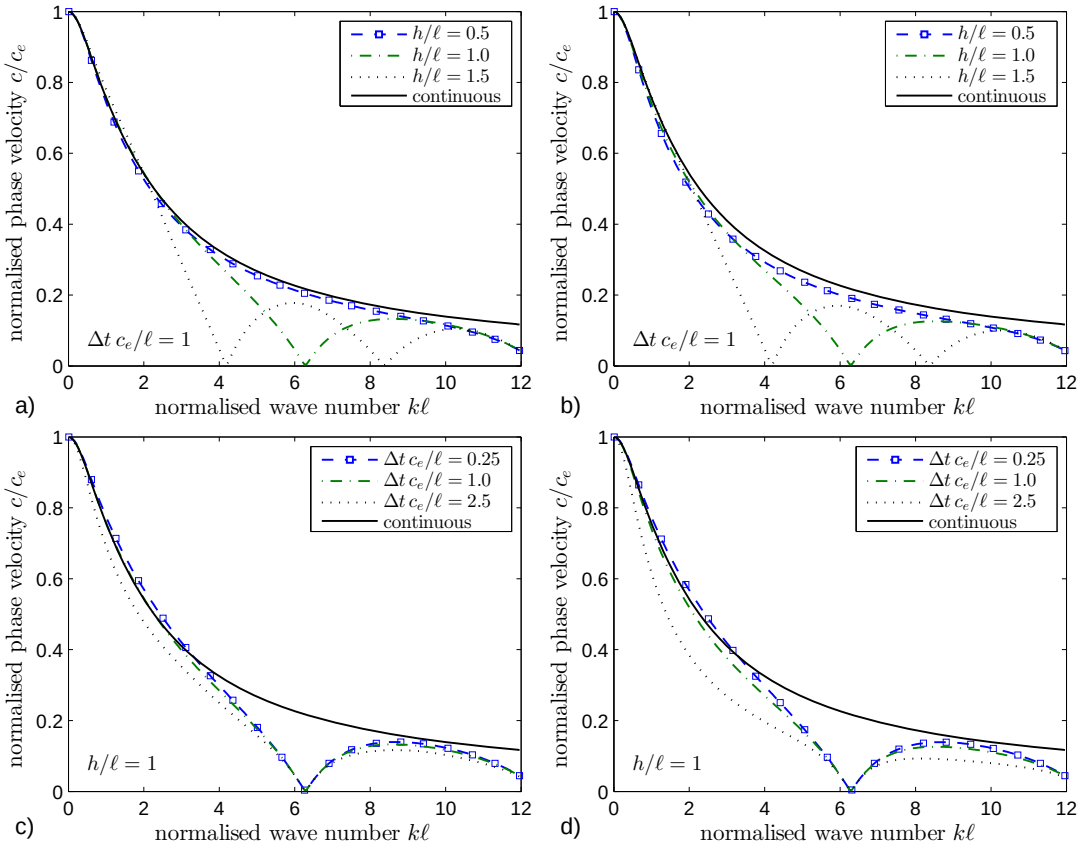

Figure 2. Normalised phase velocity *versus* normalised wave number as expressed by Eq. (35) for $r_\alpha = 2$ and $r_\beta = 0.5$: a), c) linear acceleration scheme ($\beta_n = 1/6$); b), d) constant acceleration scheme ($\beta_n = 1/4$)

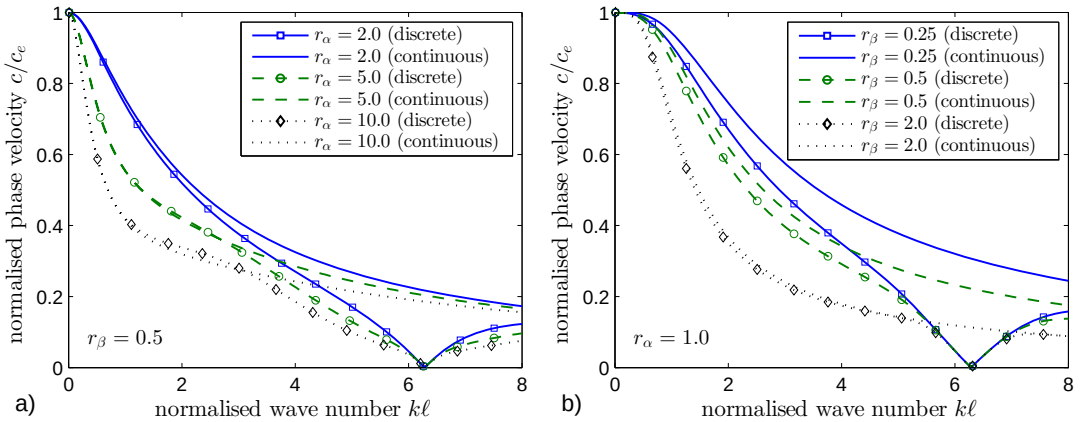

Figure 3. Normalised phase velocity *versus* normalised wave number as expressed by Eq. (35) for element size $h/\ell = 1$, time step $\Delta t c_e/\ell = 1$ and constant acceleration scheme ($\beta_n = 1/4$)

length scale are adopted, the requirements on the discretisation are less stringent to assure a certain accuracy of the numerical solution.

The curves of Figs. 2 and 3 are very useful because they facilitate the choice of the numerical discretisation parameters. Once the length scale parameters are calibrated for a given physical problem (which gives indications on r_α and r_β), the range of wave numbers that need to be simulated

DOI: 10.1002/nme

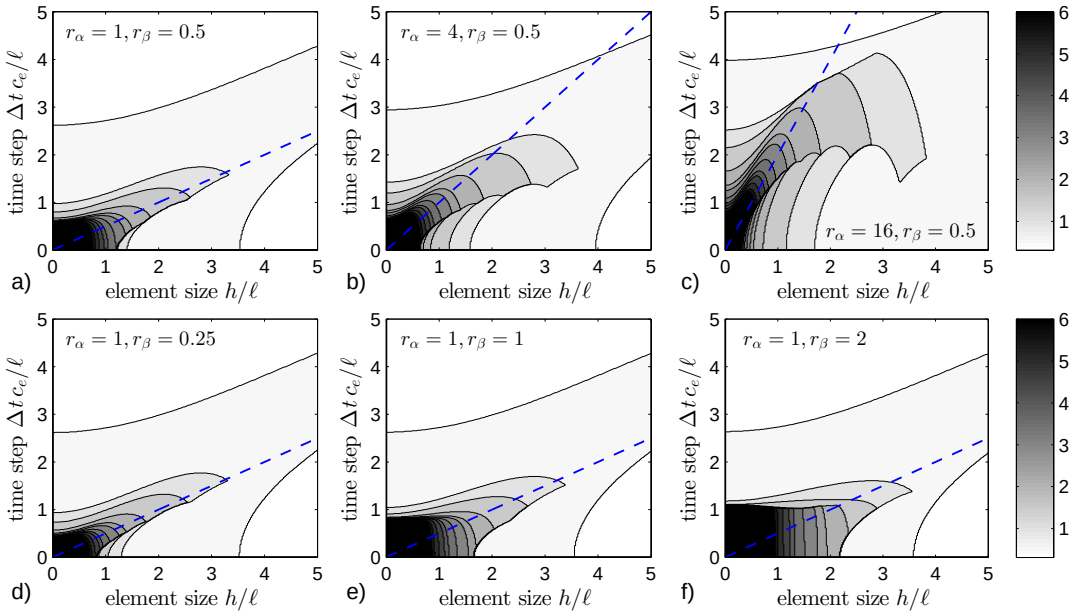

Figure 4. Contour plot of wave numbers that are captured with less than 5% error for constant acceleration scheme ($\beta_n = 1/4$) and for different ratios between the length scale parameters—dashed lines indicate optimal time step calculated according to Eq. (36)

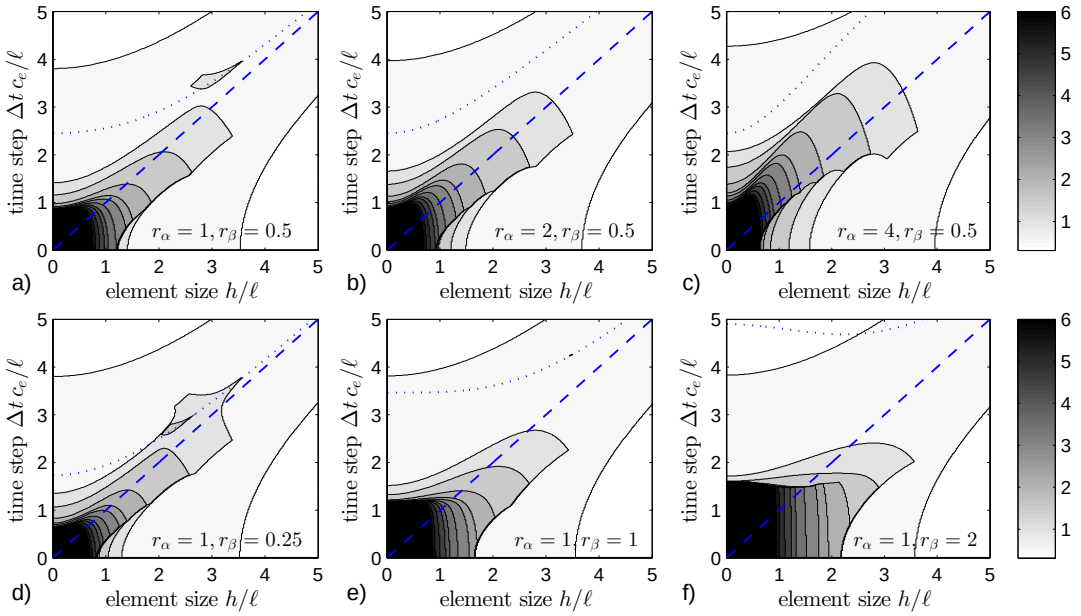

Figure 5. Contour plot of wave numbers that are captured with less than 5% error for linear acceleration scheme ($\beta_n = 1/6$) and for different ratios between the length scale parameters—dashed lines indicate optimal time step according to Eq. (38), dotted lines indicate critical time step according to Eq. (24)

accurately should be selected, and a fixed tolerance error of the discrete dispersion curve compared to the continuum dispersion curve established. On the basis of the latter choices, the optimal element size and time step can be identified a priori so that, for the range of wave numbers of interest, the discrete dispersion curve deviates less than the fixed tolerance from the continuum dispersion curve. Following this rationale, for a range of (dimensionless) element sizes and time steps we

DOI: 10.1002/nme

have computed the first (dimensionless) wave number for which the relative error of the discrete dispersion curve as compared to the continuum dispersion curve is no more that 5%. In Figs. 4 and 5 we report the contour plot of the computed wave numbers for the constant acceleration scheme and for the linear acceleration scheme, respectively. These graphs serve to indicate which wave numbers are captured accurately (within the 5% tolerance) with a given set of element size and time step and for a given set of length scale parameters. For example, from Fig. 4 b) it is noted that for $r_\alpha = 4$ and $r_\beta = 0.5$ if a unitary element size and a unitary time step are adopted as discretisation parameters, the wave numbers that are captured accurately are approximately $k\ell \approx 4$ (cf. with Fig. 3 a)). This means that if wave numbers larger than $k\ell = 4$ are to be simulated accurately, a more refined discrete model should be adopted by reducing the element size and the time step accordingly. Moreover, it can be seen that the element size and the time step should be selected proportionally. For example, focusing the attention on Fig. 4 a), if the spatial discretisation is such that $h/\ell = 2$, the best time step that should be selected is approximately $\Delta c_e/\ell \approx 1$ so that wave numbers up to $k\ell \approx 2$ are captured accurately. Refining the time step further for fixed element size $h/\ell = 2$ would lead to reduce the range of wave numbers that are described accurately, and thus would worsen, instead of improving as one would normally expect, the numerical prediction. The same result is obtained if, vice versa, for a fixed time step the element size were refined beyond a certain value. Therefore, the two discretisation parameters should be balanced according to an optimal ratio that depends on the length scale parameters. By inspection of Fig. 4 a), b), c) where for a fixed r_β we vary the r_α ratio, it can be seen that a reasonable choice of the time step for the constant acceleration scheme is (cf. [9])

$$\Delta t \approx \frac{h\sqrt{r_\alpha}}{2c_e}. \tag{36}$$

The relation described in Eq. (36) is reported as a dashed line in the contour plots of Fig. 4. On the other hand, the effect of the β-length scale is described in Fig. 4 d), e), f) where for a fixed r_α we vary the r_β ratio. The r_β ratio widens the range of element sizes and time steps for which a given accuracy is achieved, rather than modifying the slope of the optimal ratio between the two discretisation parameters. As already noted when discussing the results of Fig. 3 b), this implies that for fixed discretisation parameters a higher accuracy is achieved for increasing values of the r_β ratio or, equivalently, that for large β values the requirements on the discretisation can be made less stringent to attain a certain accuracy of the numerical solution.

Similar considerations can be made for the linear acceleration scheme, whose relevant results are reported in Fig. 5. As in the previous case, the optimal time step should be selected proportionally to the element size so that spatial and time discretisation are balanced. However, since the linear acceleration scheme is only conditionally stable, the chosen time step must be smaller than the critical time step given by Eq. (24). By looking at the profiles of the critical time step depicted in Fig. 1 a), it seems reasonable to compute an upper bound value for the time step according to the asymptotic slope of the Δt_{crit} curves that, for the linear acceleration scheme, is given by

$$m = \lim_{h\to\infty} \frac{\partial \Delta t_{\text{crit}}}{\partial h} = \frac{1}{c_e} \tag{37}$$

from which the optimal value for the time step is

$$\Delta t = m\, h = \frac{h}{c_e}. \tag{38}$$

As can be seen from Fig. 5, the upper bound value given by Eq. (38) (straight line reported in dashed) never exceeds or intersects the critical time step curve (24) (reported in dotted line). Therefore, the recommendation on the time step given by Eq. (38) leads to an effective combination between accuracy and stability: it preserves stability for the all the possible values of the element size h/ℓ, but at the same time it yields much more accurate results than the critical time step (24) for small values of the element size as illustrated in Fig. 5.

DOI: 10.1002/nme

7. NUMERICAL EXAMPLES

In this Section, the guidelines discussed above are verified numerically. Using the finite element implementation introduced in Section 2, wave propagation is examined in a one-dimensional bar as well as in a two-dimensional body. Different numerical parameters are explored to cover a broad range of examples, including discretisation parameters and material length scale coefficients. For simplicity, a uniform element size h and a uniform time step Δt are adopted throughout as discretisation parameters. Moreover, a unitary γ coefficient is assumed for all the numerical examples, so that the r_α and r_β ratios coincide with the actual values of the α and β length scale coefficients.

7.1. One-dimensional bar

As a first example, dispersive wave propagation in a simple one-dimensional bar is simulated. With reference to the test set-up shown in Fig. 6, we consider a bar having length $L = 100\,\mathrm{m}$ and cross-sectional area $A = 1\,\mathrm{m}^2$. The bar is fixed at the right hand end and subjected to a compressive unit-pulse at its left hand end, that is, a force expressed by $F = F_0\,\delta(t)$, with $\delta(t)$ the Dirac delta and $F_0 = 1\,\mathrm{N}$ the unit-pulse applied at $t = 0$. The material parameters of the bar are the Young's modulus $E = 1\,\mathrm{N/m}^2$, the mass density $\rho = 1\,\mathrm{kg/m}^3$ and the internal length scale $\ell = 1\,\mathrm{m}$.

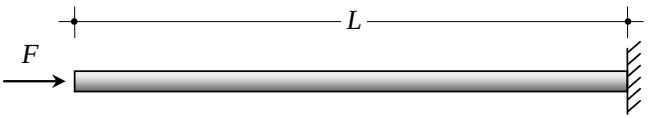

Figure 6. One-dimensional dynamic bar problem: geometry, loading and boundary conditions

In Fig. 7 a series of finite element meshes combined with proportionally scaled time steps are used to investigate the convergence of the numerical solution upon refinement. The assumed material length scale ratios are $r_\alpha = 4$ and $r_\beta = 0.5$. Two time integration algorithms have been employed, namely the implicit Newmark constant acceleration scheme and the explicit 4,5-Runge-Kutta algorithm. A reference solution for the bar problem is computed using a finite element mesh of 2000 elements and the Newmark constant acceleration scheme with $\Delta t = 0.05\,\mathrm{s}$. When refining the element size, the corresponding time step is calculated according to Eq. (36). Due to the choice of the length scale coefficients and material parameters, the optimal time step according to Eq. (36) is such that $h/\Delta t = 1\,\mathrm{m/s}$. From Fig. 7 it can be seen that the smaller wave numbers (i.e. the longer wave lengths) travel faster than the lower wave numbers as predicted by the analytical dispersion curve (11) for $\alpha > \gamma$. This holds for both the microscopic displacements u^m and the macroscopic displacements u^M, although in general the latter profile is smoother than the former owing to Eq. (2b) that relates the two displacement fields. Upon refinement both the displacements converge rapidly towards the reference solution for both the time integration methods. The two time integration methods create opposite errors with respect to the reference solution due to the fact that the implicit (explicit) schemes generally provide a lower (upper) bound value for the frequency of the exact solution. By comparing the numerical solutions of the two integration methods, the implicit method seems to be more accurate on the higher frequencies (around the tail of the wave) than the Runge-Kutta method, whereas the explicit method tends to behave in the opposite way and captures the front of the wave more accurately for equal time step.

Convergence upon refinement towards the reference solution is achieved only if element size and time step are refined proportionally. It is counterproductive to decrease either element size or time step without decreasing the other simultaneously. By keeping the same material length scale parameters as above, we consider a coarse solution obtained with $h = 2\,\mathrm{m}$ for the spatial discretisation and the constant acceleration scheme with $\Delta t = 2s$ for the time discretisation. We investigate the effect of either sole element size refinement or sole time step refinement. In Fig. 8 we report the profiles of the macroscopic displacements u^M when the element size is refined by a factor 4 and 16 for fixed time step (Fig. 8 a)), and when the time step is refined by a factor 4 and 16

DOI: 10.1002/nme

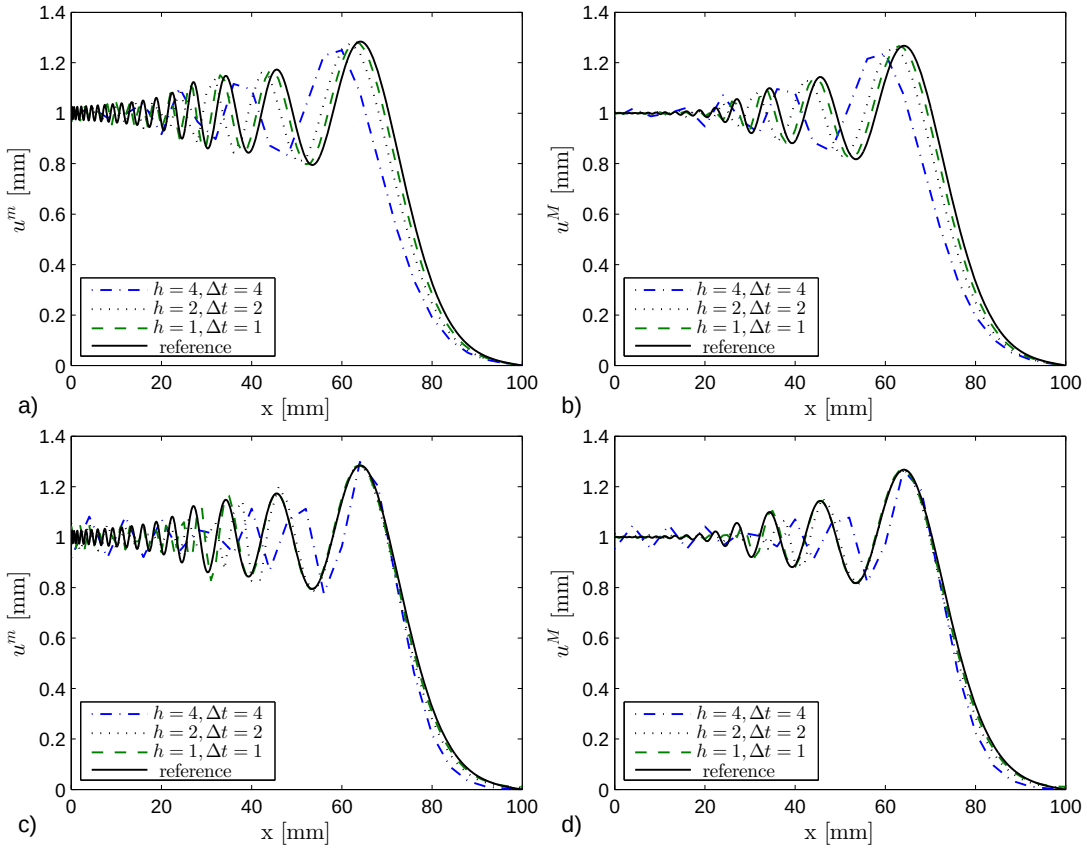

Figure 7. Dispersive wave propagation along the bar of Fig. 6 at $t = 80s$—convergence upon proportional element size/time step of the micro-displacements u^m and macro-displacements u^M: a), b) implicit Newmark constant acceleration scheme; c), d) explicit Runge-Kutta (4,5) algorithm

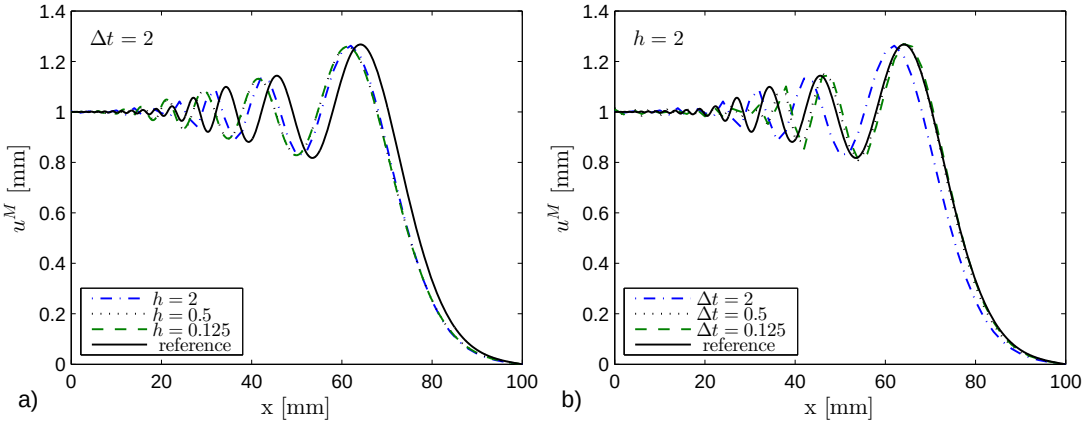

Figure 8. Wave propagation along the bar depicted in Fig. 6 at $t = 80s$: a) effect of sole element size refinement for fixed time step; b) effect of sole time step refinement for fixed element size

for fixed element size (Fig. 8 b)). In either case the numerical solution converges towards a profile that is different from the reference solution, which indicates that such refinement strategies are not effective.

DOI: 10.1002/nme

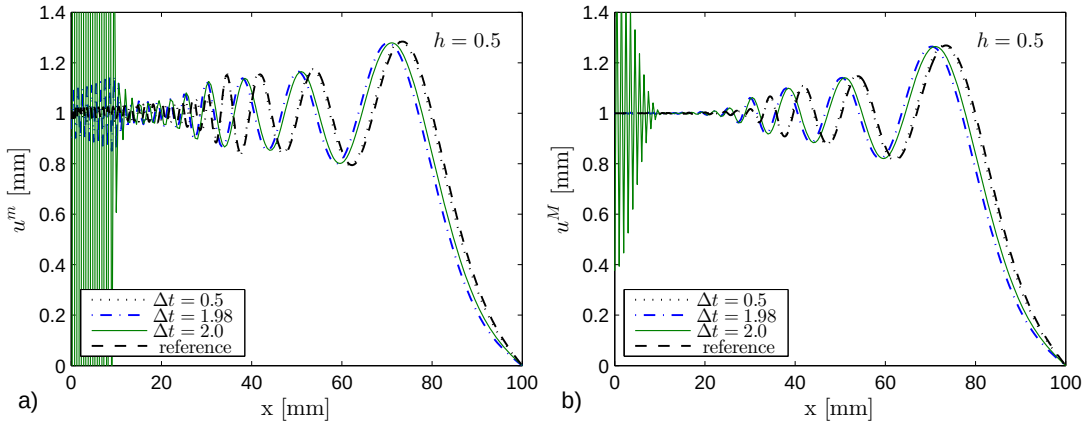

Figure 9. Role of the critical time step $\Delta t \approx 1.98s$ in the linear acceleration scheme—displacements profiles for the bar depicted in Fig. 6 at $t = 90s$: a) microscopic displacements; b) macroscopic displacements

In conditionally stable algorithms numerical instability becomes manifest when the time step Δt is selected larger than the critical time step Δt_{crit} as computed from Eq. (24). In such cases the solution blows up quickly at each time step. For the linear acceleration scheme and length scale ratios $r_\alpha = 4$ and $r_\beta = 0.25$, the critical time step for a mesh of 200 elements ($h = 0.5\,\text{m}$) is $\Delta t_{\text{crit}} \approx 1.981s$. In Fig. 9 we report the profiles of both the microscopic displacements u^m and macroscopic displacements u^M for $\Delta t = 0.5 < \Delta t_{\text{crit}}$, $\Delta t = 1.98 \approx \Delta t_{\text{crit}}$ and $\Delta t = 2 > \Delta t_{\text{crit}}$. It is worth noting that the optimal time step expressed by Eq. (38) for the linear acceleration scheme and for the given material parameters is $\Delta t = 0.5\,\text{s}$. The displacement profile obtained with the latter time step is indeed very close to the reference solution for both the displacement fields u^m and u^M. As soon as the time step approaches the critical value, instabilities first occur in the micro-displacement field and then are conveyed to the macro-displacement field via Eq. (2b) (compare Fig. 9 a) and b) for $\Delta t = 1.98$). As already noted in [9], instabilities first occur in the higher wave numbers that, for the selected length scale parameters, are the slower wave components and, thus, concentrate around the tail of the wave.

7.2. Two-dimensional plate in plane strain

In this second example, propagation of body waves in a two-dimensional plate is examined. With reference to the test set-up shown in Fig. 10, we consider a square plate having side $L = 1\,\text{m}$. The plate is constrained through sliding boundary conditions on the four sides as indicated in Fig. 10.

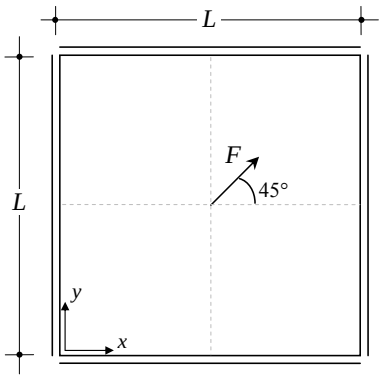

Figure 10. Two-dimensional dynamic problem: geometry, loading and boundary conditions

DOI: 10.1002/nme

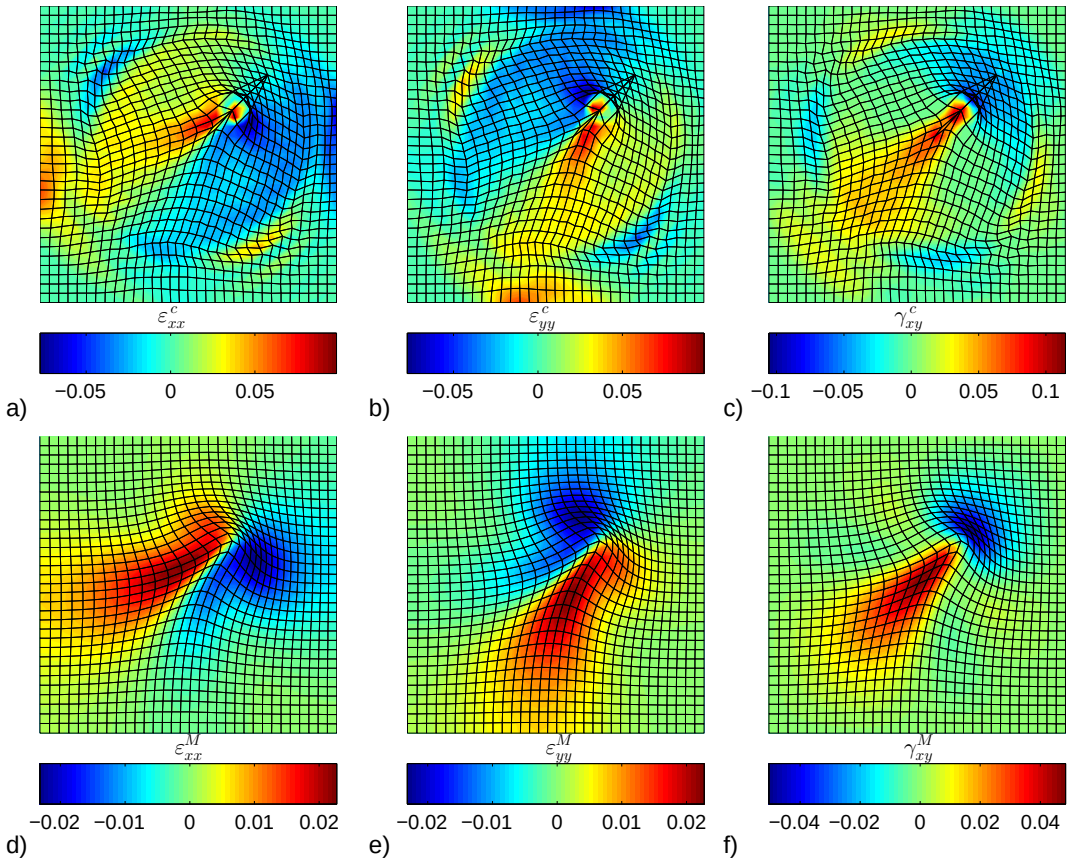

Figure 11. Two-dimensional dynamic problem sketched in Fig. (10)—contour plot, reported onto the deformed shape of the plate, of strain components at $t = 0.05s$ for mesh 32×32: a), b), c) results of classical elasticity; d), e) f) results of gradient elasticity

Propagation of body waves is triggered by a point load F applied at the centre of the specimen and forming a $45°$ angle to the x axis. The force is expressed as $F = F_0\,U(t)$, where $F_0 = \sqrt{2}\,\mathrm{N}$ is a constant stepforce at time $t = 0$ and the function $U(t)$ represents the Heaviside unit-step function. The plate is assumed to be in a plane strain configuration with the following material parameters: Young's modulus $E = 100\,\mathrm{N/m^2}$, Poisson's ratio $\nu = 0.25$, mass density $\rho = 1\,\mathrm{kg/m^3}$ and internal length scale $\ell = 0.05\,\mathrm{m}$. The values of the length scale ratios for this example are $r_\alpha = 4$ and $r_\beta = 2$.

Uniform meshes of four-noded bilinear quadrilateral elements are used. The Newmark constant acceleration scheme is employed for the time integration. As suggested in [9], the time step Δt is computed through a heuristic generalisation of Eq. (36) to two dimensions, in which the one-dimensional bar velocity of classical elasticity c_e is replaced by the compressive wave velocity c_p (cf. Section 3).

Singularities are expected in classical elasticity at the position where the point load is applied. We investigate the removal of singularities of the proposed formulation of gradient elasticity as well as the validity of the aforementioned recommendations for selecting discretisation parameters for two-dimensional cases. The results of the gradient elasticity model are reported in Fig. 11 and compared to the classical elasticity solution for a mesh consisting of 32×32 square elements. Contour plots of the macroscopic strain components are reported onto the deformed shape of the plate at time $t = 0.05s$, which is approximately equal to the time for the wave front to propagate from the centre of the specimen to the edges of the domain. The same scaling factor is used to magnify the deformed shapes of classical and gradient elasticity. As can be seen, a smooth profile of the displacements as

DOI: 10.1002/nme

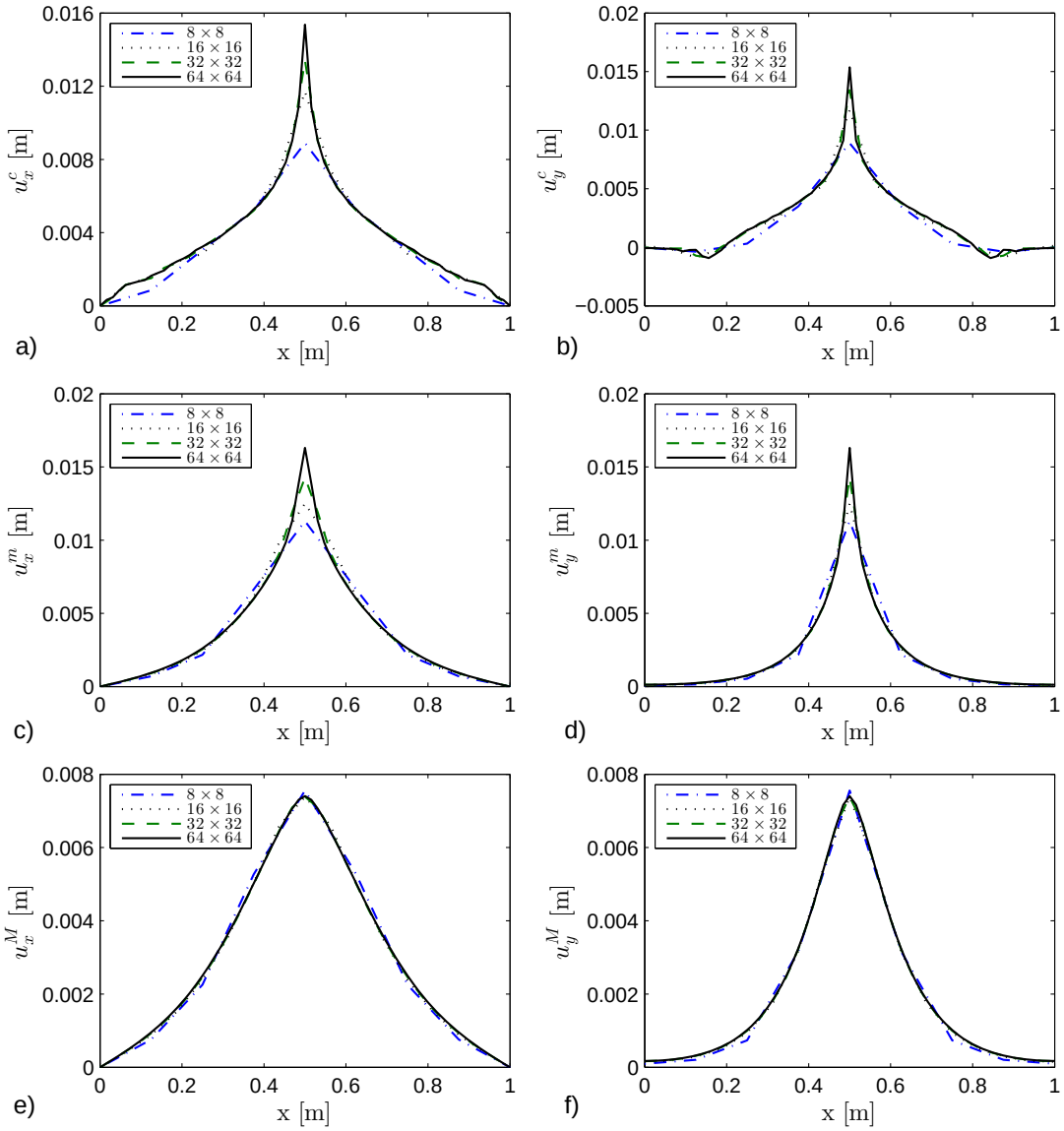

Figure 12. Two-dimensional dynamic problem sketched in Fig. (10)—profile of the displacements along the section $y = L/2$ at $t = 0.05s$: a), b) classical elasticity displacements; c), d) microscopic displacements; e), f) macroscopic displacements

well as of the strain components is achieved by the gradient elasticity model, whereas the classical elasticity results exhibit a singularity at the centre of the specimen.

To assess the removal of singularities more in-depth, we perform a mesh refinement study by using 8×8, 16×16, 32×32 and 64×64 square elements of size h. The displacement profiles along the section $y = L/2$ are reported in Fig. 12. It can be seen that singularities are detected not only in classical elasticity, but also in the microscopic displacements and strains of the gradient elasticity where unbounded peaks are found at the point $x = L/2$. Conversely, singularities disappear in the macroscopic displacement field (and, consequently, in the macroscopic strains as shown in Fig. 11). This aspect has already been clarified in [4, 8]: the differential equation that relate the macroscopic displacements to the microscopic displacements ($u_i^M - \gamma\ell^2 u_{i,nn}^M = u_i^m$) can be rewritten as an equivalent integral nonlocal relation [19] in which the u_i^M variables are interpreted as the weighted (nonlocal) average of the u_i^m variables in a certain finite neighbourhood. Therefore,

DOI: 10.1002/nme

singularities in the microscopic displacements are eliminated at the macroscale level of observation when u_i^m are mapped into the volume-averaged variables u_i^M. By inspection of Fig. 12 e), f), it is observed that the macroscopic displacements u^M are free of singularities and converge towards a unique solution upon mesh refinement. Furthermore, the displacement profiles pertaining to the four analysed meshes are actually very close to each other, which indicates, at least from a qualitative point of view, that the guidelines established for the 1D case can be applied to 2D examples.

8. CONCLUDING REMARKS

In this contribution, we have discussed a few computational aspects of a recently developed gradient elasticity model for dynamics. The proposed model incorporates three gradient terms, namely a strain gradient and two micro-inertia contributions, accompanied by three length scale parameters. The relative magnitudes between the three length scales are adjusted by three coefficients (α, β, γ) introduced in the formulation. Finite element implementation of this model has already been discussed in [10]. The computational aspects examined in this paper concern spatial and time discretisation details.

Dispersion analysis with reference to two-dimensional body waves has been performed to find analytical dispersion curves for compressive and shear waves. It has been found that these two dispersion curves have the same shape, whereby the strain gradient term accelerates while the micro-inertia terms decelerate the higher wave numbers compared to the lower wave numbers. The discretised equations of the higher-order continuum are then analysed more in-depth. Since a diagonally lumped mass matrix would cancel the higher-order effects, there would be no computational advantages in using an explicit time integration, whereas implicit methods (e.g. the Newmark scheme) are preferable because of accuracy and stability reasons. Therefore, we have investigated some computational aspects regarding the discretised equations in which the Newmark family is employed for the time integration. Firstly, stability aspects are analysed for conditionally stable variants of the Newmark family. It has been illustrated how the critical time step depends on the three length scale parameters of the model. Secondly, accuracy aspects are investigated by comparing the analytical dispersion curve of the higher-order continuum with that of the discretised medium. Once the length scale parameters for a given physical problem are calibrated and once the significant range of wave numbers that need to be simulated accurately is identified, the discretisation parameters can be selected a priori so that the discrete dispersion curve differs less than a fixed tolerance error from the continuum dispersion curve. In light of this, some guidelines have been established to select optimal values for the discretisation parameters that balance computational efficiency and numerical accuracy. The validity of these guidelines has been verified numerically by exploring the wave propagation in a few simple examples.

REFERENCES

1. Aifantis EC. On the role of gradients in localization of deformation and fracture. *International Journal of Engineering Science* 1992; **30**:1279–1299.
2. Altan B, Aifantis EC. On some aspects in the special theory of gradient elasticity. *Journal of the Mechanical Behavior of Materials* 1997; **8**: 231-282.
3. Askes H, Aifantis EC. Gradient elasticity theories in statics and dynamics - a unification of approaches. *International Journal of Fracture* 2006; **139**:297-304.
4. Askes H, Aifantis EC. Gradient elasticity in statics and dynamics: an overview of formulations, length scale identification procedures, finite element implementations and new results. *International Journal of Solids and Structures* 2011; **48**:1962-1990.
5. Askes H, Bennett T, Aifantis EC. A new formulation and $\mathscr{C}^0$-implementation of dynamically consistent gradient elasticity. *International Journal for Numerical Methods in Engineering* 2007; **72**:111-126.
6. Askes H, Metrikine AV. One-dimensional dynamically consistent gradient elasticity models derived from a discrete microstructure. Part 2: Static and dynamic response. *European Journal of Mechanics – A/Solids* 2002; **21**:573–588.
7. Bažant ZP, Jirásek M. Nonlocal integral formulations of plasticity and damage: survey of progress. *Journal of Engineering Mechanics* 2002; **11**:1119–1149.
8. Bennett T, Gitman I, Askes H. Elasticity theories with higher-order gradients of inertia and stiffness for the modelling of wave dispersion in laminates. *International Journal of Fracture* 2007; **148**:185–193.

DOI: 10.1002/nme

9. Bennett T, Askes H. Finite element modelling of wave dispersion with dynamically consistent gradient elasticity. *Computational Mechanics* 2009; **43**:815–825.
10. De Domenico D, Askes H. A new multi-scale dispersive gradient elasticity model with micro-inertia: Formulation and $\mathscr{C}^0$-finite element implementation. *International Journal for Numerical Methods in Engineering* 2016, DOI: 10.1002/nme.5222.
11. Engel G, Garikipati K, Hughes TJR, Larson MG, Mazzei L, Taylor RL. Continuous/discontinuous finite element approximations of fourth-order elliptic problems in structural and continuum mechanics with applications to thin beams and plates, and strain gradient elasticity. *Computer Methods in Applied Mechanics and Engineering* 2002; **191**:3669–3750.
12. Fuschi P, Pisano AA, De Domenico D. Plane stress problems in nonlocal elasticity: finite element solutions with a strain-difference-based formulation. *Journal of Mathematical Analysis and Applications* 2015; **431**:714–736.
13. Germain P. The Method of Virtual Power in Continuum Mechanics. Part 2: Microstructure. *SIAM J. Appl. Math.*, 1973; **25(3)**:556-575.
14. Godio M, Stefanou I, Sab K, Sulem J. Dynamic finite element formulation for Cosserat elastic plates. *International Journal for Numerical Methods in Engineering* 2015; **101**:992–1018.
15. Hughes TJR. *The Finite Element Method: Linear Static and Dynamic Finite Element Analysis*. Dover, NY, USA. 2000.
16. MathWorks. Matlab. R2012b. Computer software, http://www.mathworks.com/.
17. Maugin GA, Metrikine AV. (Eds.). *Mechanics of Generalized Continua One Hundred Years After the Cosserats*. Springer, New York. 2010.
18. Newmark NM. A method of computation for structural dynamics. *Journal of Engineering Mechanics ASCE* 1959;85:67–94.
19. Peerlings RHJ, de Borst R, Brekelmans WAM, de Vree JHV, Spee I. Some observations on localisation in non-local and gradient damage models. *European Journal of Mechanics A/Solids* 1996; **15**:937–953.
20. Polizzotto C, Fuschi P, Pisano AA. A nonhomogeneous nonlocal elasticity model. *European Journal of Mechanics A/Solids* 2006; **25**: 308–333.
21. Ru CQ, Aifantis EC. A simple approach to solve boundary-value problems in gradient elasticity. *Acta Mechanica* 1993; **101**:59–68.
22. Warren J, Yarnell J, Dolling G, Cowley R. Lattice dynamics of diamond. *Physical Review* 1967; **158**:805–808.
23. Yarnell J, Warren J, Wenzel R, Koenig S. Phonon dispersion curves in bismuth. *IBM Journal of Research and Development* 1964; **8**:234–240.
24. Yarnell J, Warren J, Koenig S. Experimental dispersion curves for phonons in aluminium. In: *Lattice Dynamics - Proceedings of an International Conference*, Wallis RF (Eds.), Pergamon Press 1965; 57–61.
25. Zervos A. Finite elements for elasticity with microstructure and gradient elasticity. *International Journal for Numerical Methods in Engineering* 2008; **73**:564–595.
26. Zervos A, Papanicolopulos SA, Vardoulakis I. Two finite element discretizations for gradient elasticity. *Journal of Engineering Mechanics* 2009; **135**:203–213.